THE JOURNAL OF BIOLOGICAL CHEMISTRY VOL. 288, NO. 5, pp. 2994–3002, February 1, 2013

Burial of the Polymorphic Residue 129 in Amyloid Fibrils of Prion Stop Mutants*[S]

Received for publication, September 28, 2012, and in revised form, November 26, 2012 Published, JBC Papers in Press, December 3, 2012, DOI 10.1074/jbc.M112.423715

Lukasz Skora[‡1], Luis Fonseca-Ornelas[‡1], Romina V. Hofele[‡1], Dietmar Riedel[‡], Karin Giller[‡], Jens Watzlawik[§], Walter J. Schulz-Schaeffer[§], Henning Urlaub[‡¶], Stefan Becker[‡], and Markus Zweckstetter[‡‖2]

From the [‡]Max Planck Institute for Biophysical Chemistry, 37077 Göttingen, the [§]Prion and Dementia Research Unit, Department of Neuropathology and the [¶]Department of Clinical Chemistry, University Medical Center Göttingen, 37075 Göttingen, and the [‖]German Center for Neurodegenerative Diseases (DZNE), 37077 Göttingen, Germany

Background: In human prion diseases, the phenotype is modified by a methionine/valine polymorphism at codon 129.
Results: Prion stop mutants have a conserved amyloid core comprising residue 129.
Conclusion: The polymorphic residue 129 is buried in the amyloid core structure.
Significance: The data support a critical role of the methionine/valine 129 polymorphism in human prion diseases.

Misfolding of the natively α-helical prion protein into a β-sheet rich isoform is related to various human diseases such as Creutzfeldt-Jakob disease and Gerstmann-Sträussler-Scheinker syndrome. In humans, the disease phenotype is modified by a methionine/valine polymorphism at codon 129 of the prion protein gene. Using a combination of hydrogen/deuterium exchange coupled to NMR spectroscopy, hydroxyl radical probing detected by mass spectrometry, and site-directed mutagenesis, we demonstrate that stop mutants of the human prion protein have a conserved amyloid core. The 129 residue is deeply buried in the amyloid core structure, and its mutation strongly impacts aggregation. Taken together the data support a critical role of the polymorphic residue 129 of the human prion protein in aggregation and disease.

Misfolding of the natively α-helical prion protein (PrP^C)[3] into a β-sheet-rich isoform is related to various human diseases such as Creutzfeldt-Jakob disease and Gerstmann-Sträussler-Scheinker syndrome collectively known as transmissible spongiform encephalopathies (1). The form of disease is determined by two prion types (2), which are a cross species phenomenon (3). Prion types are characterized by differences in stability against denaturing agents, different proteinase K-cleavage sites, and different forms of prion aggregate deposits (3). These differences were attributed to distinct prion conformations (4). In humans, a methionine/valine polymorphism at codon 129 of the prion protein gene contributes in determining disease phenotypes (2). Although both prion types can be formed with each polymorphism at codon 129, methionine shows a strong association with prion type 1 and valine with prion type 2 (5). Homozygosity at this position predominates in sporadic Creutzfeldt-Jakob disease, where up to 89% of patients of large epidemiological studies had either Met/Met or Val/Val at codon 129 (6). It has also been demonstrated that to achieve a more efficient prion transmission in human PrP-transgenic mice models, both the inoculum and the mouse should bear the same amino acid at position 129 (7).

Although the high-resolution structures of PrP^C from many species are well described (8), little is known about the structure of PrP^{Sc}. X-ray fiber diffraction showed that infectious prions have cross-β structure, confirming that prions can form amyloid (9). Antibody mapping studies suggested that when PrP^C is converted into PrP^{Sc}, a conformational rearrangement occurs in the region comprising residues 90–176 (10). Mass spectrometric analysis of hydrogen-deuterium exchange of brain-derived PrP^{Sc} suggested that prion protein conversion involves refolding of the entire region from residues ~80–90 to the C terminus (11). Electron microscopy of two-dimensional crystals of the 27–30-kDa infectious fragment, PrP27–30, suggested that PrP amyloid fibrils might consist of stacked trimers of left-handed β-helices with the core formed by residues 89–140 (12–14).

Characterization of PrP^{Sc} at high resolution is currently not possible. Therefore, a variety of studies have investigated the structure of amyloid fibrils produced *in vitro* from recombinant prion protein. Mass spectrometry-coupled exchange experiments of amyloid fibrils of human prion protein (humPrP) comprising residues 90–231 indicated strong solvent protection in the region encompassing residues ~160–230 (15). In contrast, for mouse PrP(23–231), residues 24–98 and 182–212 were protected (16). Hydrogen exchange measurements by mass spectrometry and NMR spectroscopy of mouse PrP(89–143) bearing a P101L mutation identified a high level of protection from solvent exchange for residues 102–109 and 117–136 (17). In addition, molecular dynamics simulations provided models for the conformation of PrP in prions (18).

* This work was supported by the VolkswagenStiftung (Grant ZN1294 to W. J. S.-S.), the Deutsche Forschungsgemeinschaft (Heisenberg scholarship to M. Z., ZW 71/2-2 and 3-2; Grant SFB 860 to M. Z., R. V. H., and H. U., INST 186/859-1), and the European Community's Seventh Framework Programme FP7/2009 under Grant Agreement 238316.
[S] This article contains supplemental Figs. S1 and S2.
[1] These authors contributed equally to this work.
[2] To whom correspondence should be addressed: German Center for Neurodegenerative Diseases (DZNE) and Max Planck Institute for Biophysical Chemistry, Am Fassberg 11, 37077 Göttingen, Germany. E-mail: markus.zweckstetter@dzne.de.
[3] The abbreviations used are: PrP, prion protein; PrP^C, cellular prion protein; PrP^{Sc}, scrapie form of prion protein; humPrP, human PrP; HSQC, heteronuclear single quantum coherence; H/D, hydrogen/deuterium.

Hereditary prion diseases include C-terminally truncated variants of the prion protein, Y145*X*, Q160*X*, Y226*X*, and Q227*X*, where *X* indicates the truncation site (see Fig. 1*A*). Although a single experiment to transmit human 145stop mutant prions to mice failed (19), the stop mutants provide a particularly valuable model for studying misfolding of prion protein (20, 21) as they: (i) lack the normally present glycosylphosphatidylinositol anchor and are secreted into the intercellular medium, which appears to favor fibrillization and aggregation (21, 22); (ii) show *in vivo* prion deposits in the form of amyloidogenic plaques or plaque-like aggregates, like other prion diseases (23); and (iii) aggregate under nondenaturing conditions *in vitro* (20, 22). Previously, we showed that the β-sheet content is highly similar in amyloid fibrils of the Y145*X* and Q160*X* prion stop mutants (22), and solid-state NMR spectroscopy revealed extended β-sheet conformation in the 112–140 region (24–26). Here we investigated the importance of the polymorphic residue 129 for the formation and structure of amyloid fibrils of human prion stop mutants. Using a combination of hydrogen/deuterium (H/D) exchange coupled to NMR spectroscopy, hydroxyl radical probing detected by mass spectrometry, and site-directed mutagenesis, we demonstrate that the valine/methionine residue 129 is deeply buried in the amyloid core of the stop mutants, supporting its critical role in aggregation and disease.

EXPERIMENTAL PROCEDURES

Protein Expression and Purification—Plasmids encoding Q160*X* and N174*X* were expressed in *Escherichia coli* BL21(DE3) by using M9 minimal medium with [^{15}N]NH_4Cl (1 g/liter) as the only nitrogen source and as required [$^{13}C_6$]glucose (4 g/liter), to obtain uniformly ^{15}N- or ^{13}C,^{15}N-labeled protein, and purified according to Ref. 27. Variants of humPrP(108–143) with purity exceeding 95% were obtained from EZBiolab.

Aggregation of Q160X and N174*X* into Amyloid Fibrils—Aggregation of Q160*X* and N174*X* was started by transferring protein solutions into a phosphate buffer (50 mM potassium phosphate, pH 6.5) (22). The reaction was carried at 25 °C without agitation, and fibril formation was monitored using a thioflavin T fluorescence assay.

Aggregation of humPrP(108–143)—Variants of lyophilized humPrP(108–143) were dissolved at a concentration of 0.35 mM with ice-cold 25 mM Tris buffer, pH 7.5, 0.02% sodium azide and dialyzed overnight against 500 ml of 25 mM Tris, pH 7.5, 0.02% sodium azide at 4 °C in a 500–1000-Da molecular mass cut-off dialysis membrane. The peptide was filtered through a 0.22-μm Millipore filter. Concentration was adjusted to 0.15 mM in a 500-μl final volume, and the solution was incubated at 12 °C in low binding protein 1.5-ml Eppendorf tubes. After different incubation times, a 20-μl aliquot of the sample was mixed with 1 ml of the thioflavin T assay solution (0.1 mM thioflavin T in 100 mM NaH_2PO_4, 140 mM NaCl, pH 8.5), incubated 5 min at room temperature and transferred to a 10-mm cuvette. The fluorescence emission was measured between 460 and 600 nm on a Varian Cary Eclipse fluorescence spectrophotometer (Agilent Technologies) with excitation at 442 nm at 20 °C.

Quantification of Aggregate Formation by UV Absorbance—To have a second measure for aggregate formation of different variants of humPrP(108–143), aggregates were collected after 2.7 and 24 h of incubation by centrifugation at 16,000 × *g* for 30 min at 4 °C. Subsequently, the pellet was resuspended in 100 μl of 25 mM Tris HCl, pH 7.5, and diluted in a 1:5 ratio in 7.5 M guanidine hydrochloride, 25 mM NaH_2PO_4, pH 6.5. Peptide concentrations were determined by UV absorption at 280 nm.

Electron Microscopy (EM)—The sample was bound to carbon-coated grids and stained with 1% uranyl acetate. Pictures were taken at 72,000× magnification at a CM 120 with a 2048 × 2048 pixel TemCam (Tietz) in spotscan mode.

NMR-detected H/D Exchange—Fibrils were collected by centrifugation (10,000 × *g* for 5 min) and washed 3–4 times with 50 mM phosphate buffer (pH 6.5) to remove residual monomeric protein or low molecular weight oligomers. To initiate exchange, the pellet was resuspended in D_2O buffer (0.1% formic acid in D_2O, pD 2.5) and incubated at 4 °C for 3 and 7 days. The samples were then immediately frozen in liquid nitrogen and lyophilized. For the NMR experiments, lyophilized proteins were resolubilized in ice-cold solution of 2 M guanidinium thiocyanate in 50% H_2O, 50% D_2O, pD 2.5, and a series of ^{1}H,^{15}N heteronuclear single quantum coherence (HSQC) spectra was recorded over a period of 24 h to follow the back-exchange process (28). NMR spectra were acquired at 278 K on a Bruker Avance 900 MHz spectrometer equipped with a 5-mm triple resonance cryogenic probe head. Experiment time was ~23 min, and the dead time for sample preparation and acquisition setup was 15 min. NMR data were processed and analyzed using NMRPipe (29). For nonresolvable residues within the octarepeat region, protection levels were calculated using averaged intensities. Signals originating from residues Gly-30, Trp-31, Gly-35, Arg-37, Tyr-38, Tyr-49, Gly-53, Gly-55, Trp-57, Met-109, Lys-110, Met-112, Leu-125, Ile-138, and Tyr-145 were overlapping in the denaturing condition. As signal overlap might distort the analysis and lead to false protection factors, these residues were not included into the analysis. Exchange curves were fitted to Equation 1 using IgorPro 5.01

$$I/I_0 = A1 + A2 \times \exp(A3 \times t) \quad \text{(Eq. 1)}$$

where I_0 is the signal intensity observed in the first HSQC spectrum after dissolution, and *A*1–*A*3 are fitting variables.

NMR Resonance Assignment—Sequential backbone assignment of humPrP mutants in fibril dissolving buffer was obtained from three-dimensional HACANNH, HNCACB, and HNN experiments (30, 31) recorded at 278 K on a Bruker Avance spectrometer operating at 900 MHz and equipped with a 5-mm triple resonance cryo probe. The samples used for resonance assignment contained typically 0.4 mM ^{13}C,^{15}N-labeled variant humPrP in 2 M guanidinium thiocyanate, 90% H_2O, 10% D_2O, pH 2.5. Due to severe signal overlap in the octarepeat region, only 89 resonances for 123 non-proline residues of human humPrP(23–159) were observed in two-dimensional ^{1}H,^{15}N HSQC spectra of the denatured monomer. 64 of these resonances could be assigned unambiguously, whereas the rest could only be located to the octarepeat region.

Measurement of Diffusion Coefficients—The molecular weight of the amyloid fibrils was estimated using NMR pulsed-

field gradient methods experiments (32). 10 mg of unlabeled fibrils were placed in a rotor, and diffusion coefficients were measured using the LED pulse sequence with bipolar gradients (33). Spectra were recorded on a Bruker Avance 900-MHz spectrometer equipped with a 4-mm high-resolution magic angle spinning probe. The sample was spun at 7.2 kHz, total diffusion time was $D = 100$ ms, and gradient pulse length $d = 3$ ms. Sine-shaped gradients were used, and their strength was incremented in 16 steps from $g = 0.07–0.48$ G/mm. The diffusion coefficients were calculated by fitting the intensity decay curves (see Fig. 1*C*) with the equation

$$I/I_0 = \exp[-D(\gamma dg)^2(D - d/3 - t/2)] \qquad \text{(Eq. 2)}$$

where γ is the gyromagnetic ratio of the ^{1}H nucleus, and $t = 200$ μs is the delay for gradient switching. For molecular weight estimation, 1,4-dioxane (88 Da) and bovine serum albumin (66 kDa) were used as internal and external references.

Mass Spectrometry (MS)— humPrP(108–143) was probed in the monomeric and fibrillar state by chemically generated hydroxyl radicals, as described in Ref. 34. 70 μl of 50 μM sample were added to an Eppendorf tube containing 10 μl of 13 mM Fe-EDTA (Sigma-Aldrich and Merck, respectively) solution and 10 μl of 0.2 M sodium ascorbate (Sigma-Aldrich) solution, both in 50 mM Na_2HPO_4, pH 6.5 buffer. For control purposes, a 17-μl aliquot was transferred to 40 μl of quenching buffer (2 M Tris, pH 7.2, Prolabo). Finally, 10 μl of 3% v/v H_20_2 (Sigma-Aldrich) were added to the Fenton mixture to start the reaction. At 10, 60, 150, and 300 s, 17-μl aliquots were removed and transferred to new Eppendorf tubes containing 40 μl of quenching buffer.

To disassemble the probed peptides prior to further analysis, samples were dissolved in 200 μl of acetonitrile. The total volume was reduced to ~20 μl. Subsequently, 150 μl of 100 mM Tris, 10 mM $CaCl_2$ buffer and 0.5 μg of chymotrypsin (Roche Applied Science) were added, and digestion was allowed to proceed overnight at 25 °C. The digested samples were desalted with C8 (3M) STAGE tips (35).

Nano-liquid Chromatography Separation and MS Analysis— For LC-MS/MS analyses, samples were dissolved in 30 μl of sample solvent (5% v/v acetonitrile, 1% v/v formic acid). 5 μl were injected onto a nano-liquid chromatography system (Agilent 1100 series, Agilent Technologies) including an ~2-cm-long, 150-μm inner diameter C18 trapping column in-line with an ~15-cm-long, 75-μm inner diameter C18 analytical column (both packed in-house, C18 AQ 120 Å 5 μm, Dr. Maisch GmbH, Ammerbuch, Germany). Peptides were loaded on the trapping column at a flow rate of 10 μl/min in buffer A (0.1% formic acid in H_2O, v/v) and subsequently eluted and separated on the analytical column with a gradient of 7.5–37.5% buffer B (95% acetonitrile, 0.1% formic acid in H_2O, v/v) with an elution time of 37 min and a flow rate of 300 nl/min.

Online electrospray mass ionization-MS was performed with an LTQ-Orbitrap Velos instrument (Thermo Scientific), operated in data-dependent mode using a TOP10 method. MS scans were recorded in the m/z range of 350–1600. The 10 most intense ions were selected for subsequent MS/MS. Both precursor ions as well as fragment ions were scanned in the Orbitrap. Fragment ions were generated by higher energy collision dissociation activation (normalized collision energy = 40) and recorded from $m/z = 100$. As precursor ions as well as fragment ions were scanned in the Orbitrap, the resulting spectra were measured with high accuracy (<5 ppm) both in the MS and in the MS/MS level.

Determination of Oxidized Sites—Data analysis was performed using MaxQuant 1.1.1.14 (36). Database search was performed against humPrP(108–143) with Andromeda (37) considering a total of 14 variable modifications: hydroxylation (+16 Da) in His, Val, Met, Leu, Tyr, Arg, Pro, Ile, Phe; dioxidation (+32 Da) of Met, Tyr, Phe; deguanidination (−43 Da) in Arg; and ring opening (−22) in His. The oxidation levels at any given time point were calculated on a per-residue basis. By making use of extracted ion chromatograms, obtained with Xcalibur (10 ppm tolerance), the ratios of oxidized to nonoxidized peptides in which a specific residue is involved were determined according to Ref. 38 and as illustrated below for Met-112

$$\frac{I_{\mathrm{KHM(O)AGAAAAGAVVGGKGGY}} + I_{\mathrm{KHM(O)AGAAAAGAVVGGKGGY(O)}}}{I_{\mathrm{KHMAGAAAAGAVVGGKGGY}} + I_{\mathrm{KHM(O)AGAAAAGAVVGGKGGY}} + I_{\mathrm{KHM(O)AGAAAAGAVVGGKGGY(O)}}} \qquad \text{(Eq. 3)}$$

where O indicates the oxidized residue. Because ionization efficiencies of modified and unmodified species are similar, but not identical, the results need be interpreted in a relative context (*i.e.* fibrillar *versus* monomeric states). For quantification of peptides that contain several modifications in different combinations that lead to the same m/z value (termed isobaric oxidized peptides), we made use of the fact that these elute at different retention times from the LC into the mass spectrometer (ranging from 1 to 9 min with respect to the nonoxidized peptide). To the same purpose, only the most abundant charge state of each peptide was considered.

Error Calculation—Two independently prepared fibril samples and two monomeric samples were measured and used for error calculation, and the error informed corresponds to the S.E. It should be noted that the sum of the intensities corresponding to different combinations of oxidized residues (the case for most methionines) lead to higher uncertainties, which stresses the need for the results to be interpreted in a relative context.

RESULTS

Size Estimation of humPrP(23–159) Fibrils—To characterize the molecular weight of humPrP(23–159) fibrils (Fig. 1*B*), we have used pulsed-field gradient methods (32) combined with high-resolution magic angle spinning (Fig. 1*C*). High-resolution magic angle spinning averages out NMR signal broadening caused by inhomogeneity in magnetic field anisotropy and thus allows detection of flexible regions in aggregates, whereas NMR-based pulsed field gradient methods provide an estimate of the diffusion coefficient of aggregates. To take into account the nonspherical shape of fibrils and contribution from rotational diffusion, the equations described by Perrin (39) were applied to calculate the corresponding diffusion constant of a spherical molecule of the same molecular weight. For this calculation, the average diameter and length of the fibrils were estimated from EM micrographs as 15 and 500 nm, respec-

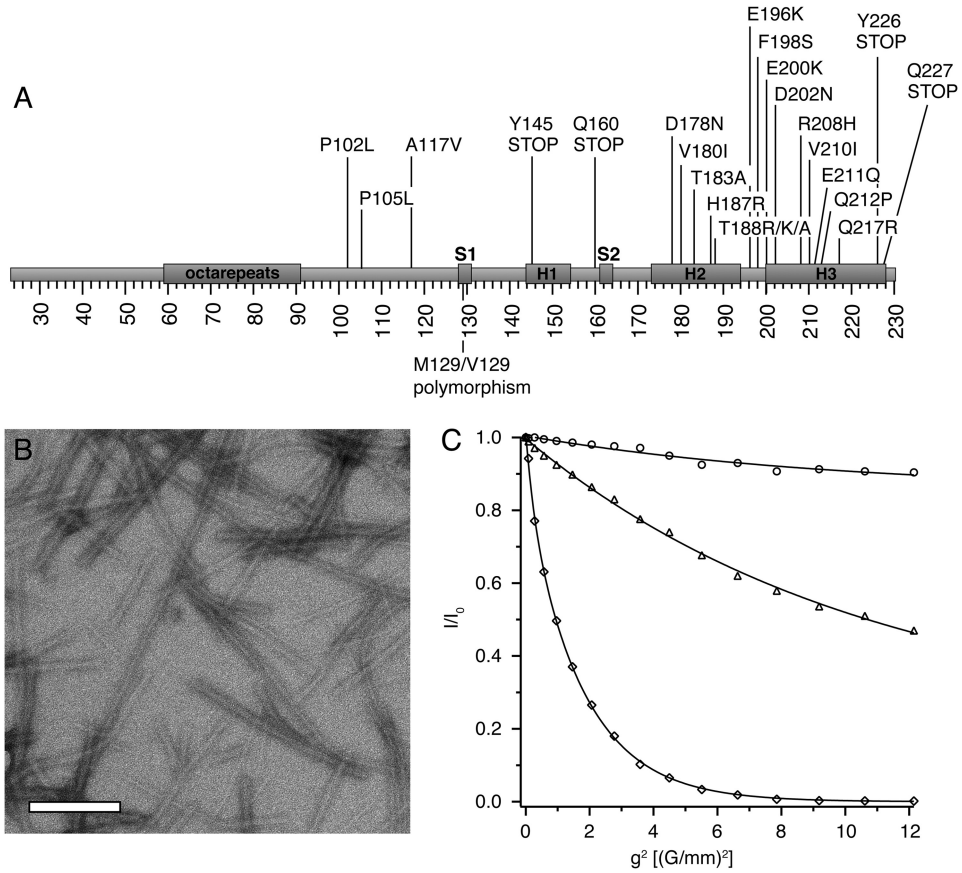

FIGURE 1. **Amyloid fibrils of humPrP(23–159).** *A*, schematic representation of native secondary structure elements and point mutations found in the human prion protein. *B*, electron micrographs of mature fibrils. The *white bar* indicates 200 nm. *C*, decay of NMR signal intensity under pulsed field gradients recorded for humPrP(23–159) fibrils (*circles*), bovine serum albumin (*triangles*), and 1,4-dioxane (*diamonds*). The measured diffusion coefficient of fibrils of humPrP(23–159) was 2.6×10^{-11} m^2/s.

tively. Using the Stokes-Einstein relation, the molecular weight of humPrP(23–159) fibrils was estimated to be in the order of 4 MDa.

Solvent Protection in the Fibrillar State—The solvent accessibilities of single residues in amyloid fibrils (Fig. 2) of the hereditary stop mutant Q160*X* were probed using NMR-detected H/D exchange (40). To allow detection by liquid-state NMR and at the same time preserve the H/D exchange pattern, fibrils that had been exposed to H/D exchange were rapidly converted to monomers in a 2 M solution of guanidinium thiocyanate in 50% H_2O, 50% D_2O (28). Back-exchange was then monitored in the denatured state by a series of two-dimensional ^1H,^{15}N HSQC spectra (Fig. 2). Neglecting back-exchange before and during the first HSQC after dissolution, the intensity ratio is 1.0 for an amide proton, for which the protection level in the fibril is 50%, and reaches a minimum of 0.5 for an amide proton with a 100% protection level in the fibrillar state.

To allow a residue-specific analysis of the H/D exchange, an assignment of the denatured protein in the dissolving buffer was required. Due to severe signal overlap in the octarepeat region, 89 distinct resonances for 123 non-proline residues of human humPrP(23–159) were observed in two-dimensional ^1H,^{15}N HSQC spectra of the denatured monomer. Sequence-specific backbone assignment was obtained for 64 of these resonances from a set of standard three-dimensional HACANNH, HNCACB, and HNN experiments (30, 31). The rest could only be located to the octarepeat region. Based on the sequence-specific resonance assignment, a solvent protection map was constructed that revealed back-exchange ratios of more than 1.2 for the segments 23–108 and 143–173 (Fig. 3*A*). In the central domain comprising residues 109–142, two regions could be distinguished: residues 109–120 and 140–142 with intermediate amide proton back-exchange ratios (exchange ratios of 1.0–1.2) and residues 121–139 with high protection values (>70%). A very similar protection map was obtained after 3 instead of 7 days of H/D exchange (Fig. 3*A*).

Methionine 129 Is Strongly Protected from Solvent Exchange—Comparison of H/D exchange profiles for individual residues (Figs. 2*B* and 3*A*) provides further insight. Firstly, within the region 109–140, Gly-119 and Ala-120 showed the most pronounced increase in signal intensity during the back-exchange process, suggesting that a turn may be formed by these residues. Secondly, the striking change in the exchange profiles from Ile-139 to His-140 points to a well defined boundary of the fibrillar core. Thirdly, residues 144–156 that form helix1 in the native structure of the human prion protein (8) showed high back-exchange ratios, comparable with the flexible N-terminal domain and suggesting that the helix1 region is highly solvent-accessible in amyloid fibrils of humPrP(23–159). Fourth, the polymorphic residue Met-129 is strongly protected from solvent exchange.

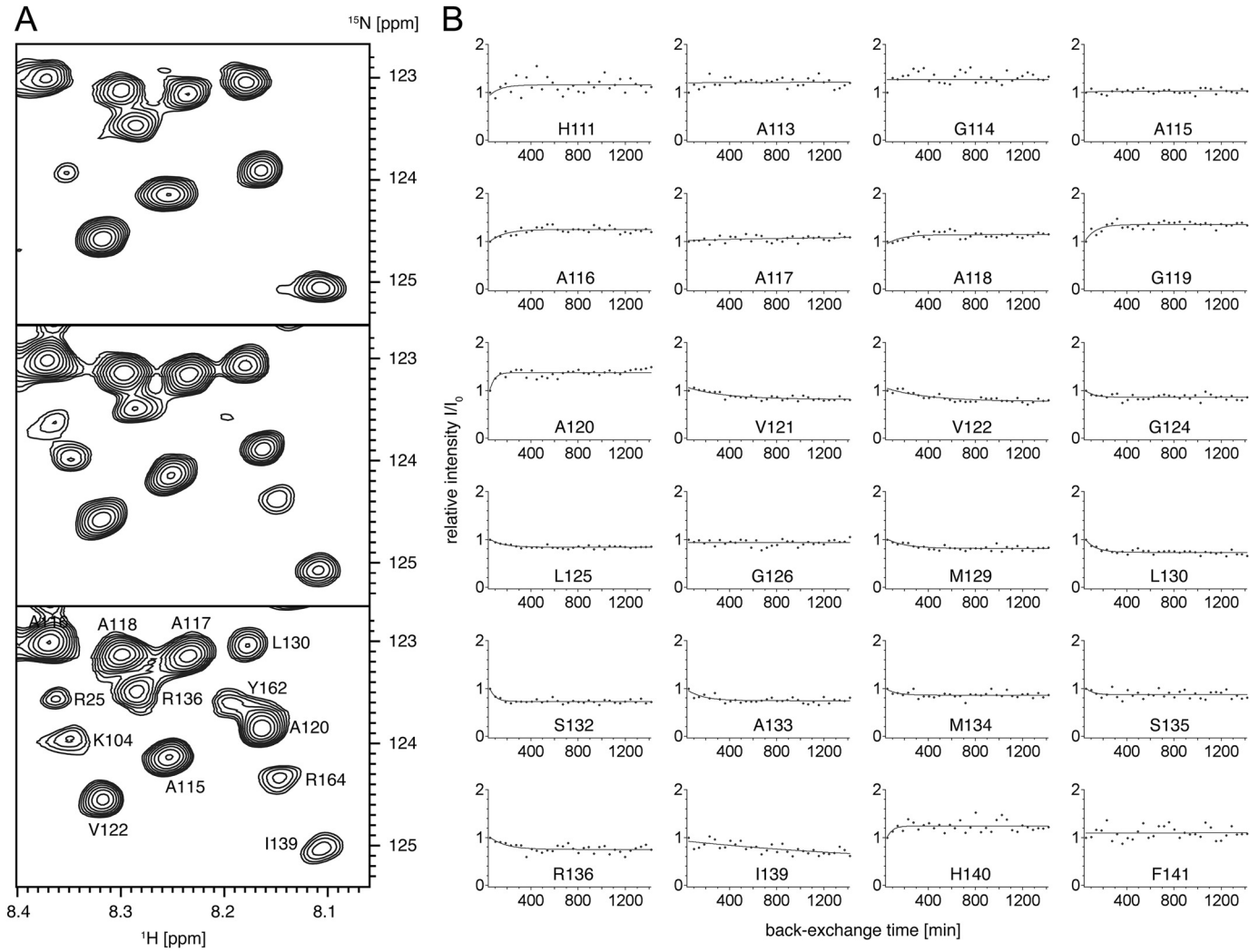

FIGURE 2. **Solvent protection in amyloid fibrils of the Q160*X* stop mutant.** *A*, excerpts from two-dimensional ^{1}H,^{15}N correlation spectra showing changes in signal intensities during the back-exchange process. The spectra were taken 1 (*top*), 6 (middle), and 24 h (*bottom*) after the dissolution of fibrils. Sequence-specific assignments are indicated. *B*, changes in signal intensities over time of individual residues in the region 111–141 due to back-exchange in the denatured monomeric state. Only data for residues that do not overlap in the two-dimensional ^{1}H,^{15}N HSQCs are shown.

A Common Amyloid Core of Human Prion Stop Mutants—To probe the structural consequences of residues ^{160}QVYY^{163}, which form β-strand 2 in the native PrP structure, we performed H/D exchange on amyloid fibrils of the designed stop mutant N174*X*. The solvent protection map of N174*X* was very similar to the exchange profile of the Q160*X* stop mutant (Fig. 3*B*). The high solvent accessibility of residues 160–170 suggested that this region is not part of the fibrillar core in the N174*X* stop mutant. In longer peptides, however, more extensive structure could be present in this sequence stretch. The combined H/D exchange data indicate that the hydrogen-bonded core of amyloid fibrils of Q160*X* and N174*X* stop mutants of the human prion protein comprises residues 121–139, flanked by residues 109–120 and 140–142.

The Side Chain of the Polymorphic Residue 129 Is Buried in the Amyloid Core—Next, we investigated the organization of single side chains in the amyloid structure of prion stop mutants using hydroxyl radical probing (Fig. 4). Hydroxyl radicals covalently modify side chains of solvent-accessible amino acids. The modifications induce a mass shift that can be detected by mass spectrometry (41). Measurements were performed for the peptide humPrP(108–143) that covers the fibrillar core of the stop mutants (Fig. 3) (24–26) and for which amyloid fibrils are morphologically similar to those of the stop mutants (Fig. 5). When compared with the stop mutants, the humPrP(108–143) peptide has two important advantages: (i) peptides obtained by solid-phase synthesis and stored as lyophilized powder are less prone to oxidation of methionine residues, a problem previously reported for recombinant prion protein (42); and (ii) the disordered N-terminal tail comprising residues 23–107 does not modulate the rate of aggregation.

Hydroxyl radical probing was applied to humPrP(108–143) in both the disordered monomer and the fibrillar state (Fig. 4 and supplemental Fig. S1). Oxidative modifications were observed for residues Met-109, Met-112, Tyr-128, Met-129, Leu-130, Met-134, Arg-136, Pro-137, Ile-138, Ile-139, His-140, and Phe-141 (Fig. 4 and supplemental Fig. S2). Other amino acid residues were not modified because of their lower reactivity or solvent accessibility. Strikingly, a pronounced reduction in oxidation was observed for the side chains of Tyr-128, Met-129, and

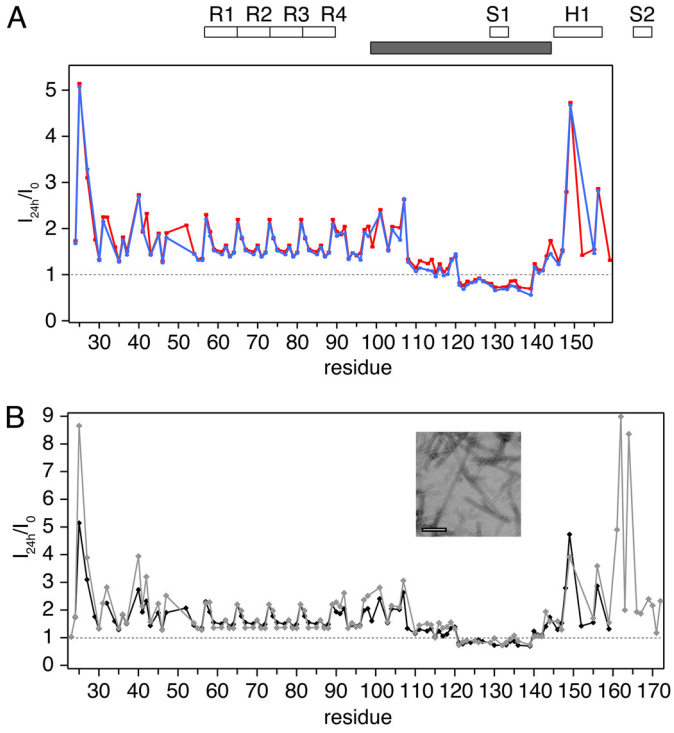

FIGURE 3. **A conserved solvent-protected core in amyloid fibrils of stop mutants of the human prion protein.** *A*, comparison of the H/D protection maps of humPrP(23–159) fibrils exchanged in D_2O for 3 days (*blue*) and 7 days (*red*). *R1–R4* are the octarepeats. Above part of the domain organization of PrpC is shown (strands S1 and S2; helix H1; repeats R1-R4). *B*, H/D protection maps of humPrP(23–159) (*black*) and humPrP(23–173) (*gray*) fibrils exchanged in D_2O for 7 days. In *A* and *B*, I_{24h} is the signal intensity after 24 h of back-exchange relative to the signal intensity I_0 observed in the first HSQC spectrum after dissolution. $I_{24h}/I_0 < 1.0$ indicates strong protection from exchange. The location of the proteinase K-resistant core is shown by a *gray bar*. Only data for nonoverlapping residues are shown. The *inset* shows an electron micrograph of humPrP(23–159) fibrils.

Leu-130 in the fibrillar state (Fig. 4*B*). In addition, small differences in oxidation levels were present for Ile-138 and Phe-141. No changes in oxidation were observed for the side chains of Met-109, Met-112, Met-134, Arg-136, Pro-137, Ile-139, and His-140 despite the fact that the backbone amide protons of several of these residues are part of a fibrillar β-strand (24).

Position 129 Is Critical for Aggregation of Human Prion Stop Mutants—The burial of the side chain of Met-129 in the fibrillar core suggests an important role of this residue for aggregation of the prion protein. To test this hypothesis, we introduced point mutations into humPrP(108–143). Removal of the hydrophobic side chain by the substitutions M129N and M129D inhibited the aggregation of humPrP(108–143) (Fig. 5). In contrast, substitution of Met-109 by lysine did not have any effect, consistent with the location of Met-109 outside of the solvent-protected region (Fig. 3, Table 1). Importantly, substitution of Met-129 with valine reduced the lag time of fibril formation. Moreover, when mixing humPrP(108–143) with the Val-129 variant at a ratio of 1:3, the lag phase of the aggregation was in between that of the two pure peptides, whereas at an equal ratio of the two variants, aggregation was retarded when compared with the Met-129 variant alone (Fig. 5*A*). Thus, a 1:1 mixture of Met-129 and Val-129 humPrP(108–143) aggregates slower than the pure peptides at the same total concentration, suggesting that the two variants are not as active in the formation of aggregation nuclei as the pure sequences.

The importance of the 129 position for prion aggregation was further supported by seeding experiments. After 6 h of aggregation, Met-129 humPrP(108–143) amyloid fibrils were fragmented and homogenized with three 5-min sonication cycles. Three different volume/volume percentages (0.1, 1, and 5%) were used as seeds on fresh preparations of monomeric Met-129, Asn-129, and Asp-129 peptides. Regardless of the seed concentration, there was no seeding effect on either Asn-129 or Asp-129 peptides, whereas the Met-129 seed on Met-129 fresh monomer completely removed the nucleation phase (Fig. 5*D*).

DISCUSSION

Biochemical analyses of aggregated prion protein in patients with a stop codon mutation suffering from a prion disease have shown that the protein resulting from the mutated allele forms the aggregates (23, 43, 44). However, a single experiment to transmit human 145stop mutant prions to New Zealand White mice failed (19).

Using H/D exchange coupled to NMR spectroscopy, we showed that the Q160*X* and N174*X* stop mutants of the human prion protein have a common solvent-protected core (Fig. 3) that starts at residue 109 and ends at residue 142. Residues ^{160}QVYY^{163}, which form β-strand 2 in the native PrP structure, are not part of the fibrillar core of these stop mutants. In addition, residues 144–156 that form helix1 in the native structure (8) remain highly solvent-accessible in amyloid fibrils of humPrP(23–159). *In vitro* aggregated amyloid fibrils of Q160*X* and Y145*X* are morphologically similar according to electron microscopy (20, 22) and have similar proteinase K cleavage sites (22). Moreover, solid-state NMR measurements of Y145*X* located the β-sheet-rich amyloid core to residues 112–140 (24). Taken together the data suggest that their amyloid fibrils share a common structure starting at residue 109–112 and ending at residue 140–142. The identified fibril core is consistent with a major PrP fragment of ~7 kDa that was detected in amyloid fibrils purified from the 145stop mutant (43), from the 227stop mutant (44), and from Gerstmann-Sträussler-Scheinker brains and spans residues 81–82 to 144–153 (45). Moreover, the fibrillar core represents the most conserved sequence element in mammalian and nonmammalian prion proteins (46) and encompasses the peptide fragment 112–119 that is essential for the replication of the infectious agent in tissue culture (47).

Recently, some of us determined the backbone fold of amyloid fibrils of the Y145*X* stop mutant by application of the CS-Rosetta structure calculation program to experimental solid-state NMR chemical shifts (24, 48). The calculations revealed a left-handed β-helix formed by three β-strands. The Met-129 side chain is located in the beginning of the third β-strand and points inward to the hydrophobic core of the left-handed β-helix. The structural model is well supported by the solvent accessibility of individual side chains obtained by mass spectrometry. Met-129 shows a pronounced reduction of solvent accessibility in the amyloid state (Fig. 4), in line with the structural model proposed for the Y145*X* stop mutant (48).

Besides Met-129, the side chains of Tyr-128 and Leu-130 are solvent-protected in the amyloid state according to mass spectrometry (Fig. 4). In the β-helix model of the Y145*X* stop mutant, the two residues belong, together with Met-129, to a

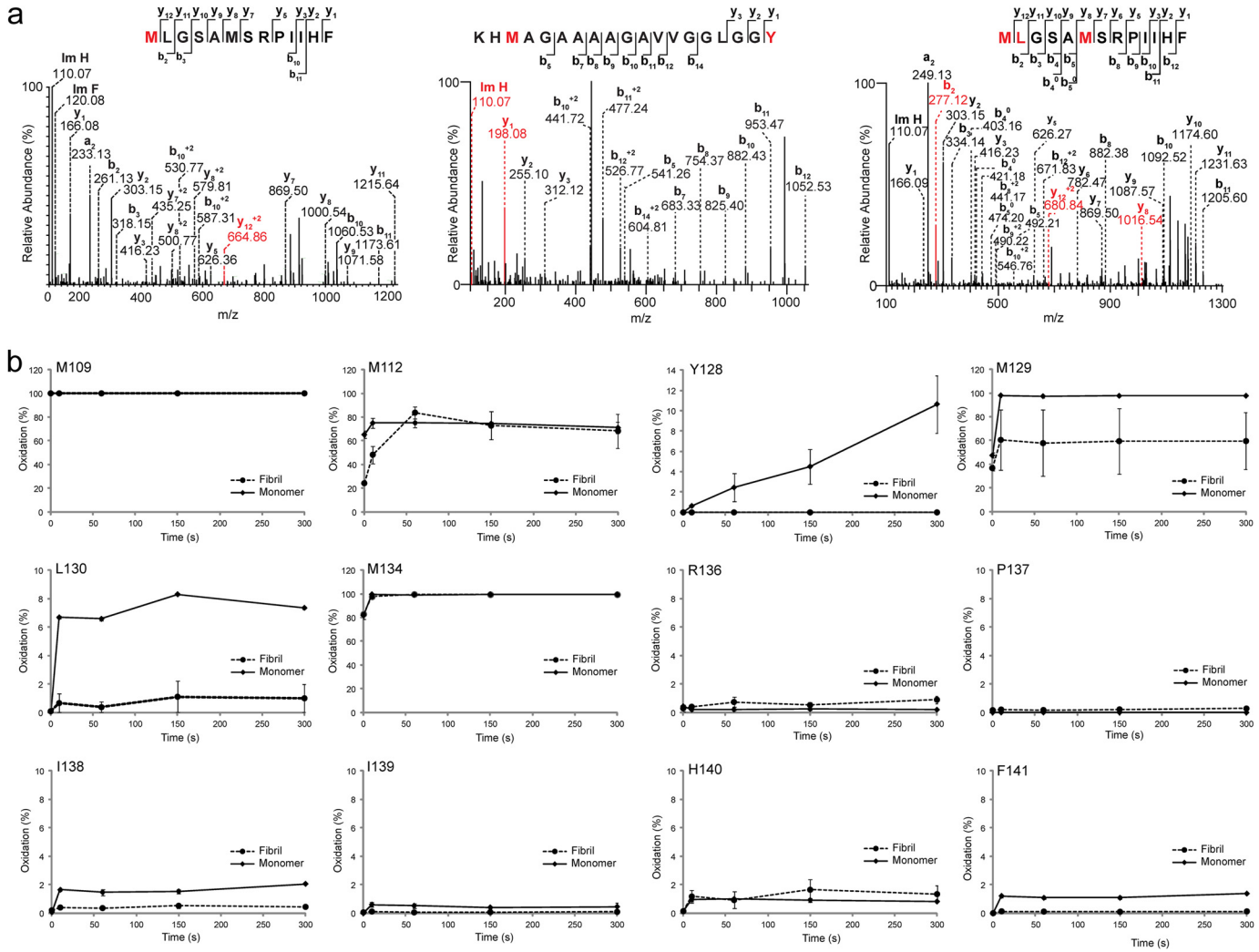

FIGURE 4. **Burial of the Met-129 side chain in amyloid fibrils of humPrP(108–143).** *A*, tandem MS spectra of oxidized humPrP(108–143). The oxidized amino acid and its corresponding fragment ions containing the modification are depicted in *red*, and *b* and *y* ions indicate fragmentation of the peptide bond conserving the charge to the N or C terminus, respectively. In the peptide MLGSAMSRPIIHF (129–141), residues Met-129, Leu-130, and Met-134 are oxidized. *B*, time-course modifications of single residues for the fibrillar (*dashed line*) and monomeric state (*solid line*). *Error bars* correspond to S.E. obtained from independent measurements on two fibrillar and two monomeric samples.

single β-strand formed by ^{128}YMLGSAMSR^{136} (48). The experimental solvent accessibilities of the ^{128}YMLGSAMSR^{136} β-strand suggest that both sides of this β-strand are protected. The side harboring the Met-129 side chain forms the hydrophobic core of the β-helix. In contrast, the side harboring Tyr-128 and Leu-130 is not protected in a single filament. A possible explanation for the solvent protection of the Tyr-128 and Leu-130 side chains in light of the β-helix model could be the pairing of two or more filaments, a hypothesis that would be supported by the dimensions of amyloid fibrils of the prion stop mutants observed by electron microscopy (22).

In humans, the disease phenotype is modified by a methionine/valine polymorphism at codon 129 of the prion protein gene in addition to the prion type. Increasing evidence suggests that changes between methionine and valine do not affect the folding or stability of the native structure, implying that its influence takes place at downstream stages in the disease. Based on the broadening of the signals of Met-129 in solid-state NMR measurements of the Y145*X* stop mutant, it was suggested that Met-129 is located in a flexible loop (24). In contrast, using a combination of H/D exchange coupled to NMR spectroscopy and hydroxyl radical probing detected by mass spectrometry, we demonstrate that the amide proton of Met-129 has slow solvent exchange in the fibrillar state and that its side chain becomes buried upon aggregation into amyloid. We therefore attribute the line broadening observed in solid-state NMR experiments for residues 121–141 (25) to dynamics between different filaments. At the same time, a high rigidity of a single PrP filament is supported by the finding that submicrosecond time scale dynamics are uniform across the amyloid core (25).

In agreement with the burial of Met-129 in the amyloid core, the presence of a valine residue at position 129 strongly enhanced aggregation of humPrP(108–143) (Fig. 5*A*). The strong effect of the Val-129 substitution might at first sight appear surprising as the Val-129 variant of humPrP(23–144) converted to amyloid fibrils only slightly faster than Met-129 in previous *in vitro* studies (49). We attribute the differences to the entropic barrier provided by the unstructured residues 23–108 thereby masking differences between different PrP variants. In support of an entropic barrier, aggregation of humPrP(23–144)

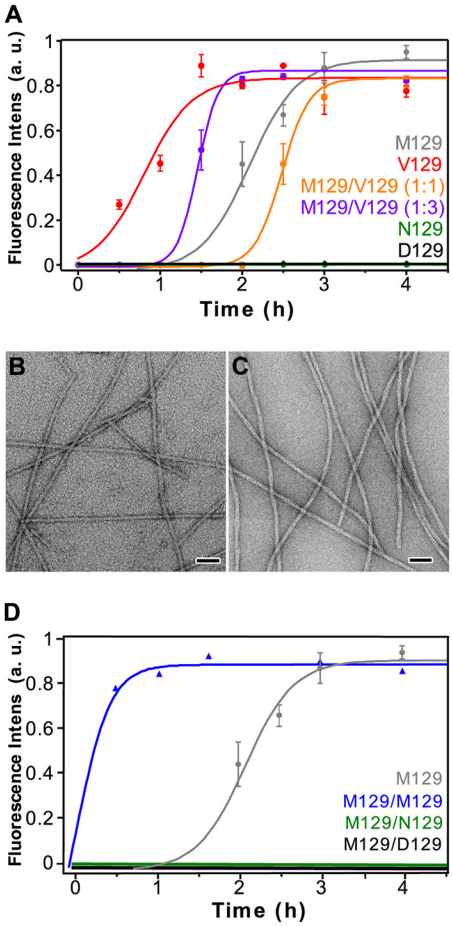

FIGURE 5. **Importance of residue 129 for aggregation of humPrP(108–143).** *A*, fibrillization kinetics of humPrP(108–143) variants. *Error bars* correspond to S.D. (at least three data sets). *B*, electron micrograph of wild-type humPrP(108–143). The average diameter was 7–9 nm. *C*, electron micrograph of M109K humPrP(108–143). The *black bar* indicates 200 nm. *D*, seeding fibrillization of Met-129, M129D, and M129N humPrP(108–143) by amyloid seeds of Met-129 humPrP(108–143). The concentration of the seed was 5%. Data for Met-129 humPrP(108–143) without seed (*gray*) were taken from *panel A*.

TABLE 1

Quantification of aggregate formation of wild-type and M109K humPrP(108–143) by centrifugation and protein quantification using UV absorbance

ThT, thioflavin T.

	2.7 h		24 h	
Peptide	% in pellet	ThT intensity	% in pellet	Tht intensity
WT	58	437.5	62	418
M109K	48	389	63	455.5

and humPrP(23–159) requires severalfold higher concentrations than humPrP(108–143) (Fig. 5*A*) (22). Importantly, both the Met-129 and the Val-129 humPrP(108–143) peptide displayed a shorter nucleation phase than their 1:1 combination modeling the heterozygous situation. Indeed, humans that are heterozygote at codon 129 of the prion protein gene are relatively protected from prion diseases, and homozygotes, either methionine or valine, are 2–4-fold more susceptible (50).

The finding that the Val-129 variant aggregates faster than Met-129 of humPrP(23–144) is in contrast to previous aggregation experiments using recombinant PrP(90–231), where methionine is more aggregation-promoting than valine (51). Besides differences in the experimental settings, an explanation may be that the C-terminally truncated mutants aggregate to a different prion type than the N-terminally truncated one. From large epidemiological studies, we know that 87% of the methionine-homozygous sporadic Creutzfeldt-Jakob disease subjects accumulate prion type 1 and 97.5% of the valine homozygous Creutzfeldt-Jakob disease subjects accumulate prion type 2 (2). Taking this into account, the observed structure, starting at 109–112 and ending at 140–142, may represent the structural motif of prion type 2.

In summary, we demonstrated that the polymorphic residue 129 is deeply buried in the amyloid core of stop mutants of the human prion protein. In line with its burial in the amyloid core structure, the identity of the 129 side chain is important for aggregation into amyloid fibrils. Our data support a critical role of the polymorphic residue 129 in the packing of protein chains into prion particles.

Acknowledgment—We thank Dr. Michael Kramer for discussions.

REFERENCES

1. Aguzzi, A., Sigurdson, C., and Heikenwaelder, M. (2008) Molecular mechanisms of prion pathogenesis. *Annu. Rev. Pathol.* **3,** 11–40
2. Parchi, P., Giese, A., Capellari, S., Brown, P., Schulz-Schaeffer, W., Windl, O., Zerr, I., Budka, H., Kopp, N., Piccardo, P., Poser, S., Rojiani, A., Streichemberger, N., Julien, J., Vital, C., Ghetti, B., Gambetti, P., and Kretzschmar, H. (1999) Classification of sporadic Creutzfeldt-Jakob disease based on molecular and phenotypic analysis of 300 subjects. *Ann. Neurol* **46,** 224–233
3. Wemheuer, W. M., Benestad, S. L., Wrede, A., Schulze-Sturm, U., Wemheuer, W. E., Hahmann, U., Gawinecka, J., Schütz, E., Zerr, I., Brenig, B., Bratberg, B., Andréoletti, O., and Schulz-Schaeffer, W. J. (2009) Similarities between forms of sheep scrapie and Creutzfeldt-Jakob disease are encoded by distinct prion types. *Am. J. Pathol.* **175,** 2566–2573
4. Parchi, P., Zou, W., Wang, W., Brown, P., Capellari, S., Ghetti, B., Kopp, N., Schulz-Schaeffer, W. J., Kretzschmar, H. A., Head, M. W., Ironside, J. W., Gambetti, P., and Chen, S. G. (2000) Genetic influence on the structural variations of the abnormal prion protein. *Proc. Natl. Acad. Sci. U.S.A.* **97,** 10168–10172
5. Schulz-Schaeffer, W. J., Giese, A., Windl, O., and Kretzschmar, H. A. (1996) Polymorphism at codon 129 of the prion protein gene determines cerebellar pathology in Creutzfeldt-Jakob disease. *Clin. Neuropathol* **15,** 353–357
6. Heinemann, U., Krasnianski, A., Meissner, B., Varges, D., Kallenberg, K., Schulz-Schaeffer, W. J., Steinhoff, B. J., Grasbon-Frodl, E. M., Kretzschmar, H. A., and Zerr, I. (2007) Creutzfeldt-Jakob disease in Germany: a prospective 12-year surveillance. *Brain* **130,** 1350–1359
7. Telling, G. C. (2011) Transgenic mouse models and prion strains. *Top Curr. Chem.* **305,** 79–99
8. Wüthrich, K., and Riek, R. (2001) Three-dimensional structures of prion proteins. *Adv. Protein Chem.* **57,** 55–82
9. Wille, H., Bian, W., McDonald, M., Kendall, A., Colby, D. W., Bloch, L., Ollesch, J., Borovinskiy, A. L., Cohen, F. E., Prusiner, S. B., and Stubbs, G. (2009) Natural and synthetic prion structure from x-ray fiber diffraction. *Proc. Natl. Acad. Sci. U.S.A.* **106,** 16990–16995
10. Paramithiotis, E., Pinard, M., Lawton, T., LaBoissiere, S., Leathers, V. L., Zou, W. Q., Estey, L. A., Lamontagne, J., Lehto, M. T., Kondejewski, L. H., Francoeur, G. P., Papadopoulos, M., Haghighat, A., Spatz, S. J., Head, M., Will, R., Ironside, J., O'Rourke, K., Tonelli, Q., Ledebur, H. C., Chakrabartty, A., and Cashman, N. R. (2003) A prion protein epitope selective for the pathologically misfolded conformation. *Nat. Med.* **9,** 893–899
11. Smirnovas, V., Baron, G. S., Offerdahl, D. K., Raymond, G. J., Caughey, B., and Surewicz, W. K. (2011) Structural organization of brain-derived mammalian prions examined by hydrogen-deuterium exchange. *Nat.*

Struct. Mol. Biol. **18,** 504–506
12. Govaerts, C., Wille, H., Prusiner, S. B., and Cohen, F. E. (2004) Evidence for assembly of prions with left-handed β-helices into trimers. *Proc. Natl. Acad. Sci. U.S.A.* **101,** 8342–8347
13. Wille, H., Govaerts, C., Borovinskiy, A., Latawiec, D., Downing, K. H., Cohen, F. E., and Prusiner, S. B. (2007) Electron crystallography of the scrapie prion protein complexed with heavy metals. *Arch Biochem. Biophys.* **467,** 239–248
14. Kunes, K. C., Clark, S. C., Cox, D. L., and Singh, R. R. (2008) Left handed β helix models for mammalian prion fibrils. *Prion* **2,** 81–90
15. Lu, X., Wintrode, P. L., and Surewicz, W. K. (2007) β-Sheet core of human prion protein amyloid fibrils as determined by hydrogen/deuterium exchange. *Proc. Natl. Acad. Sci. U.S.A.* **104,** 1510–1515
16. Nazabal, A., Hornemann, S., Aguzzi, A., and Zenobi, R. (2009) Hydrogen/deuterium exchange mass spectrometry identifies two highly protected regions in recombinant full-length prion protein amyloid fibrils. *J. Mass Spectrom* **44,** 965–977
17. Damo, S. M., Phillips, A. H., Young, A. L., Li, S., Woods, V. L., Jr., and Wemmer, D. E. (2010) Probing the conformation of a prion protein fibril with hydrogen exchange. *J. Biol. Chem.* **285,** 32303–32311
18. DeMarco, M. L., and Daggett, V. (2004) From conversion to aggregation: protofibril formation of the prion protein. *Proc. Natl. Acad. Sci. U.S.A.* **101,** 2293–2298
19. Tateishi, J., Kitamoto, T., Kretzschmar, H., and Mehraein, P. (1996) Immunohistological evaluation of Creutzfeldt-Jakob disease with reference to the type PrPres deposition. *Clin. Neuropathol* **15,** 358–360
20. Kundu, B., Maiti, N. R., Jones, E. M., Surewicz, K. A., Vanik, D. L., and Surewicz, W. K. (2003) Nucleation-dependent conformational conversion of the Y145Stop variant of human prion protein: structural clues for prion propagation. *Proc. Natl. Acad. Sci. U.S.A.* **100,** 12069–12074
21. Vanik, D. L., Surewicz, K. A., and Surewicz, W. K. (2004) Molecular basis of barriers for interspecies transmissibility of mammalian prions. *Mol. Cell* **14,** 139–145
22. Watzlawik, J., Skora, L., Frense, D., Griesinger, C., Zweckstetter, M., Schulz-Schaeffer, W. J., and Kramer, M. L. (2006) Prion protein helix1 promotes aggregation but is not converted into β-sheet. *J. Biol. Chem.* **281,** 30242–30250
23. Jayadev, S., Nochlin, D., Poorkaj, P., Steinbart, E. J., Mastrianni, J. A., Montine, T. J., Ghetti, B., Schellenberg, G. D., Bird, T. D., and Leverenz, J. B. (2011) Familial prion disease with Alzheimer disease-like Tau pathology and clinical phenotype. *Ann. Neurol* **69,** 712–720
24. Helmus, J. J., Surewicz, K., Nadaud, P. S., Surewicz, W. K., and Jaroniec, C. P. (2008) Molecular conformation and dynamics of the Y145Stop variant of human prion protein in amyloid fibrils. *Proc. Natl. Acad. Sci. U.S.A.* **105,** 6284–6289
25. Helmus, J. J., Surewicz, K., Surewicz, W. K., and Jaroniec, C. P. (2010) Conformational flexibility of Y145Stop human prion protein amyloid fibrils probed by solid-state nuclear magnetic resonance spectroscopy. *J. Am. Chem. Soc.* **132,** 2393–2403
26. Helmus, J. J., Surewicz, K., Apostol, M. I., Surewicz, W. K., and Jaroniec, C. P. (2011) Intermolecular alignment in Y145Stop human prion protein amyloid fibrils probed by solid-state NMR spectroscopy. *J. Am. Chem. Soc.* **133,** 13934–13937
27. Liemann, S., and Glockshuber, R. (1999) Influence of amino acid substitutions related to inherited human prion diseases on the thermodynamic stability of the cellular prion protein. *Biochemistry* **38,** 3258–3267
28. Cho, M. K., Kim, H. Y., Fernandez, C. O., Becker, S., and Zweckstetter, M. (2011) Conserved core of amyloid fibrils of wild type and A30P mutant α-synuclein. *Protein Sci.* **20,** 387–395
29. Delaglio, F., Grzesiek, S., Vuister, G. W., Zhu, G., Pfeifer, J., and Bax, A. (1995) NMRPipe: a multidimensional spectral processing system based on UNIX pipes. *J. Biomol. NMR* **6,** 277–293
30. Bax, A., and Grzesiek, S. (1993) Methodological advances in protein. *Acc. Chem. Res.* **26,** 131–138
31. Panchal, S. C., Bhavesh, N. S., and Hosur, R. V. (2001) Improved 3D triple resonance experiments, HNN and HN(C)N, for HN and ^{15}N sequential correlations in (^{13}C, ^{15}N) labeled proteins: application to unfolded proteins. *J. Biomol. NMR* **20,** 135–147
32. Stejskal, E. O., and Tanner, J. E. (1965) Spin diffusion measurements: spin echoes in the presence of a time-dependent field gradient. *J. Chem. Phys.* **42,** 288–292
33. Wu, D. H., Chen, A. D., and Johnson, C. S. (1995) An improved diffusion-ordered spectroscopy experiment incorporating bipolar-gradient pulses. *J. Magn. Reson. A* **115,** 260–264
34. Sharp, J. S., Becker, J. M., and Hettich, R. L. (2003) Protein surface mapping by chemical oxidation: structural analysis by mass spectrometry. *Anal. Biochem.* **313,** 216–225
35. Rappsilber, J., Ishihama, Y., and Mann, M. (2003) Stop and go extraction tips for matrix-assisted laser desorption/ionization, nanoelectrospray, and LC/MS sample pretreatment in proteomics. *Anal. Chem.* **75,** 663–670
36. Cox, J., and Mann, M. (2008) MaxQuant enables high peptide identification rates, individualized p.p.b.-range mass accuracies, and proteome-wide protein quantification. *Nat. Biotechnol.* **26,** 1367–1372
37. Cox, J., Neuhauser, N., Michalski, A., Scheltema, R. A., Olsen, J. V., and Mann, M. (2011) Andromeda: a peptide search engine integrated into the MaxQuant environment. *J. Proteome Res.* **10,** 1794–1805
38. Charvátová, O., Foley, B. L., Bern, M. W., Sharp, J. S., Orlando, R., and Woods, R. J. (2008) Quantifying protein interface footprinting by hydroxyl radical oxidation and molecular dynamics simulation: application to galectin-1. *J. Am. Soc. Mass Spectrom* **19,** 1692–1705
39. Perrin, F. (1934) Brownian motion of an ellipsoid. I. Dielectric dispersion for ellipsoidal molecules. *J. Phys. Radium* **5,** 497–511
40. Hoshino, M., Katou, H., Hagihara, Y., Hasegawa, K., Naiki, H., and Goto, Y. (2002) Mapping the core of the β_2-microglobulin amyloid fibril by H/D exchange. *Nat. Struct. Biol.* **9,** 332–336
41. Xu, G., and Chance, M. R. (2007) Hydroxyl radical-mediated modification of proteins as probes for structural proteomics. *Chem. Rev.* **107,** 3514–3543
42. Breydo, L., Bocharova, O. V., Makarava, N., Salnikov, V. V., Anderson, M., and Baskakov, I. V. (2005) Methionine oxidation interferes with conversion of the prion protein into the fibrillar proteinase K-resistant conformation. *Biochemistry* **44,** 15534–15543
43. Ghetti, B., Piccardo, P., Spillantini, M. G., Ichimiya, Y., Porro, M., Perini, F., Kitamoto, T., Tateishi, J., Seiler, C., Frangione, B., Bugiani, O., Giaccone, G., Prelli, F., Goedert, M., Dlouhy, S. R., and Tagliavini, F. (1996) Vascular variant of prion protein cerebral amyloidosis with Tau-positive neurofibrillary tangles: the phenotype of the stop codon 145 mutation in PRNP. *Proc. Natl. Acad. Sci. U.S.A.* **93,** 744–748
44. Jansen, C., Parchi, P., Capellari, S., Vermeij, A. J., Corrado, P., Baas, F., Strammiello, R., van Gool, W. A., van Swieten, J. C., and Rozemuller, A. J. (2010) Prion protein amyloidosis with divergent phenotype associated with two novel nonsense mutations in PRNP. *Acta Neuropathol* **119,** 189–197
45. Tagliavini, F., Prelli, F., Ghiso, J., Bugiani, O., Serban, D., Prusiner, S. B., Farlow, M. R., Ghetti, B., and Frangione, B. (1991) Amyloid protein of Gerstmann-Sträussler-Scheinker disease (Indiana kindred) is an 11 kd fragment of prion protein with an N-terminal glycine at codon 58. *EMBO J.* **10,** 513–519
46. Wopfner, F., Weidenhöfer, G., Schneider, R., von Brunn, A., Gilch, S., Schwarz, T. F., Werner, T., and Schätzl, H. M. (1999) Analysis of 27 mammalian and 9 avian PrPs reveals high conservation of flexible regions of the prion protein. *J. Mol. Biol.* **289,** 1163–1178
47. Hölscher, C., Delius, H., and Bürkle, A. (1998) Overexpression of nonconvertible PrP^c Δ114–121 in scrapie-infected mouse neuroblastoma cells leads to trans-dominant inhibition of wild-type PrP^{Sc} accumulation. *J. Virol.* **72,** 1153–1159
48. Skora, L., and Zweckstetter, M. (2012) Determination of amyloid core structure using chemical shifts. *Protein Sci.* **21,** 1948–1953
49. Jones, E. M., Surewicz, K., and Surewicz, W. K. (2006) Role of N-terminal familial mutations in prion protein fibrillization and prion amyloid propagation in vitro. *J. Biol. Chem.* **281,** 8190–8196
50. Palmer, M. S., Dryden, A. J., Hughes, J. T., and Collinge, J. (1991) Homozygous prion protein genotype predisposes to sporadic Creutzfeldt-Jakob disease. *Nature* **352,** 340–342
51. Tahiri-Alaoui, A., Gill, A. C., Disterer, P., and James, W. (2004) Methionine 129 variant of human prion protein oligomerizes more rapidly than the valine 129 variant: implications for disease susceptibility to Creutzfeldt-Jakob disease. *J. Biol. Chem.* **279,** 31390–31397